

## Article

# Flight Time Optimization and Modeling of a Hybrid Gasoline–Electric Multirotor Drone: An Experimental Study

Khaled Jarrah <sup>\*,†</sup>, Yazen Alali <sup>†</sup>, Alyssa Lalko <sup>†</sup> and Osamah Rawashdeh <sup>†</sup>

Department of Electrical and Computer Engineering, Oakland University, Rochester, MI 48309, USA

\* Correspondence: kjarrah@oakland.edu

† All authors contributed equally to this work.

**Abstract:** Drones have evolved rapidly over the decades, but the limited flight time inhibits multirotor drones from performing long-duration tasks. Batteries that power drones are considered an inadequate power source due to their low energy density. As gasoline is an energy-dense source, combining an electric propulsion system with gasoline engines should be considered. This paper proposes a novel hybrid multirotor drone design using two gasoline engines to provide the majority of the lift force and four electric motors to stabilize the drone. These propulsion systems have been characterized and optimized to exploit their respective advantages, which reduce the total energy consumption rate and increase flight time. Simulation and experimental results show that the hybrid gas–electric multirotor drone can achieve more than three times the flight time of the fully electric drone.

**Keywords:** hybrid drone design; energy consumption rate; thrust ratio; gasoline propulsion system



**Citation:** Jarrah, K.; Alali, Y.; Lalko, A.; Rawashdeh, O. Flight Time Optimization and Modeling of a Hybrid Gasoline–Electric Multirotor Drone: An Experimental Study. *Aerospace* **2022**, *9*, 799. <https://doi.org/10.3390/aerospace9120799>

Academic Editor: Haixin Chen

Received: 28 September 2022

Accepted: 1 December 2022

Published: 6 December 2022

**Publisher's Note:** MDPI stays neutral with regard to jurisdictional claims in published maps and institutional affiliations.



**Copyright:** © 2022 by the authors. Licensee MDPI, Basel, Switzerland. This article is an open access article distributed under the terms and conditions of the Creative Commons Attribution (CC BY) license (<https://creativecommons.org/licenses/by/4.0/>).

## 1. Introduction

Unmanned aerial vehicles (UAVs), or drones, have grown tremendously in popularity in recent years. Drones are involved in performing missions such as reconnaissance, search and rescue, surveillance, and survey of remote or dangerous locations [1]. Multirotor drones are popular for their maneuverability, vertical take-off and landing, and hovering capabilities. However, the limited flight endurance restricts multirotor drones from completing time-sensitive and long, persistent missions. This limitation is present in multirotor drones due to their reliance on batteries as their sole power source for their high efficiency, long service life, and simplicity [2]. Batteries have a low energy density, leading to short endurance and long charging time [3]. Current commercial multirotor drones can fly for around 25 min with batteries [4].

Hybrid propulsion technology, including fuel cells, solar panels, fossil fuel, supercapacitors, and battery combinations, has been an area of intense research in recent years [5]. The hybrid propulsion system combines at least two power sources in a certain way. Hybridization is mainly used in UAVs to increase drones' efficiency, extend flight time, and reduce energy consumption rates without degrading flight performance.

At present, hydrogen fuel cell drones have promising flight endurance but low power densities limit their abilities. The power density represents the power amount that the source can provide in a particular instance [6]. It has a crucial impact on the drone's performance because it controls the peak speed, altitude, rate of climbing, and load capacity [7]. On the other hand, energy density is the amount of power a source can provide within a certain period, directly affecting flight endurance. The energy densities for fuel cells and batteries are higher than the supercapacitors. Therefore, supercapacitors can offer a large amount of power for a short period, allowing the UAV to perform maneuvers requiring fast power response. However, fuel cells and batteries can provide a lower power amount than capacitors but for a longer period. Figure 1 shows the power and energy densities for different propulsion sources [8].

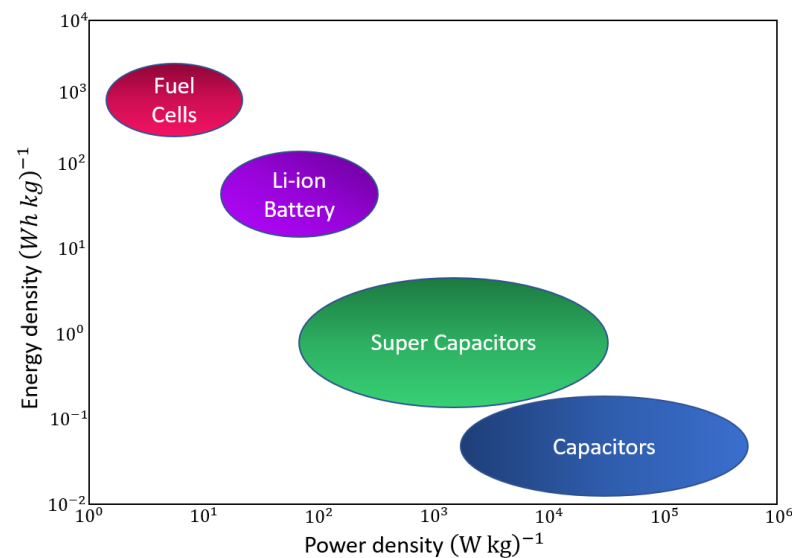


**Figure 1.** Ragone plot showing the power density vs. the energy density relative to present-day technology.

Another important source of energy is solar cells, which convert sunlight into electricity. The advantage of this technology is that the transformation process can be carried out without polluting the earth's environment [9]. However, these solar cells have lower energy and power densities compared with gasoline. Furthermore, the power obtained from the cell depends on its surface area. Therefore, solar cells are typically implemented on aircraft with wings. Even so, this poses challenges: the area of the wings of an aircraft operating only with solar cells must be larger than the area necessary to generate sufficient lift [10]. Thus, solar cells are not a promising solution to increasing the flight time of multirotor drones.

For years, batteries with electric drives have been the only propulsion system in UAVs. Electric drives have almost no power plant noise emissions except for propeller noise. They are reliable, clean, simple, and contain no flammable substances [11]. However, the energy densities for batteries are much lower than some other energy sources, such as gasoline. Thus, the flight endurances for electric UAVs are short and not suitable to perform long-duration flights. Gasoline has a very high energy density at 12.2 kWh/kg compared to lithium polymer batteries (LiPo), which are around 150–250 Wh/kg [12–16]. Therefore, harnessing gasoline to provide the lift force for the drones is a desirable solution. Using gasoline to extend the flight time of a multirotor drone is the main object of this paper.

Hence, in this paper, a hybrid multirotor prototype was designed and implemented to exploit the advantages of both gasoline and electric power sources and to balance their limitations. This study aims to determine how the addition of a low-cost commercial-of-the-shelf (COTS) gasoline propulsion system improves the flight time of an electric multirotor drone. The hybrid propulsion system was modeled and simulated to predict flight time and investigate the energy reserves required to achieve the maximum flight time. Furthermore, experimental studies were performed to evaluate the flight time and verify the simulation.

Hybrid-electric propulsion systems have three main configurations: series, parallel, and power-split configuration. Each design has its advantages and drawbacks. In the series configuration, all propellers are driven only by electric motors, and the mechanical energy of the internal combustion engines is converted into electrical energy by the generator. This configuration is relatively easy to control. However, its operating capabilities are limited and its architecture results in inefficiency and increases system weight [17]. The parallel configuration includes a single drive from each propulsion system. Both are coupled mechanically to drive the same propeller. This configuration allows for a variety of operating modes and permits higher matching to power requirements. However, this

configuration suffers from the extra mass of the coupling module and requires an advanced drive control system [18].

The power-split configuration completely separates the two propulsion systems. This is the simplest method of hybridization, but introduces some structural complexity and requires sophisticated control schemes [19]. In this paper, the prototype is constructed in the power-split configuration. Its electric and gasoline propulsion systems components independently drive their own set of propellers, and each system has its own fuel source. This setup uses minimal necessary custom parts. Furthermore, this setup is a basic form of hybridization that allows for individual characterization of both propulsion systems.

The remainder of this paper is organized as follows: We review the related work in Section 2. Section 3 presents the prototype implementation, including the flight controller modifications to accommodate the gasoline engines. The characterization process of the actuators is introduced in Section 4 to investigate their thrust output relative to their energy consumption. Section 5 discusses the minimum thrust required from each propulsion system to achieve a reliable flight performance. After that, the system model determines the recommended battery capacity and fuel volume to carry onboard in Section 6. The simulation results are verified experimentally and discussed in Section 7. Finally, Section 8 summarizes the conclusions and presents future work.

## 2. Related Work

Recently, drones have shown promise in various fields. Therefore, flight endurance is the focus of several types of research. Said research provided several techniques to increase the flight time, such as swapping [20,21], tethering [22,23], laser-beam inflight recharging [24,25], and hybridization [26–28]. Swapping is a technique that involves replacing a discharged battery with a charged one, but this technique requires stationary or mobile ground stations distributed in specific locations. In tethering, the endurance is unlimited because the flying drone will be connected directly to the power supply ground station, but this technique restricts the mobility of the drone. In the laser beam technique, flying drones receive light power through laser beams emitted from ground stations. While less restricting than tethering, this technique still limits the drone's range.

Hybridization is a technique that combines the advantages of two or more energy sources to increase flight endurance and energy usage efficiency and achieve high-performance operations. Furthermore, no ground stations are necessary as in the previous techniques. Koster et al. developed a green aircraft technology called Hyperion [29]. This 3-m aircraft includes a new hybrid gas/biodiesel–electric power train operating in internal combustion, hybrid, or electric mode. Gong et al. presented a flight test of a triple-hybrid propulsion system UAV consisting of a fuel cell, a battery, and a supercapacitor [30]. This triple hybrid propulsion system combines the performance benefits of each power source. These sources are installed in parallel to enable load sharing between each of the three power sources. Harvey et al. showed that although the application of photovoltaic cells on the aircraft caused a slight increase in weight, the addition of photovoltaic cells to the hybrid drone (fuel cell and battery) would increase the flight endurance as it saves 59% of the h<sub>2</sub> fuel [31]. Shiau et al. improved an experimental UAV flight endurance by designing a battery-backed solar power management system to supply the necessary power to the onboard electronic system components [32].

Some researchers have combined gasoline and electric power in UAVs due to the enormous endurance they can achieve with gasoline. Lu et al. introduced a novel hybrid gas–electric propulsion system for a micro triple tilt-rotor vertical take-off and landing (VTOL) prototype [33]. This UAV can operate as a parallel hybrid configuration according to the driving conditions in motor mode, engine mode, or hybrid mode. However, all energies are used directly. In other words, there are no fuel power generation processes. National Cheng Kung University developed another hybrid gas–electric drone in 2017 [34]. Preliminary tests have shown that it can fly for about 60 minutes with no payload. This research focuses on controllability and targets this amount of time. The number and

arrangement of rotors, number of batteries, thrust distribution, size, and weight of this drone significantly differs from the prototype in our study.

### 3. Prototype Implementation

The gasoline–electric hybrid drone was constructed from the Tarot 680 Pro hexacopter platform, 695 mm in diameter. First, the prototype was constructed as a fully electric quadcopter. It was characterized, and then the gasoline system was added to create the hybrid prototype. Although built for electric-only drones, the Pixhawk was suitable for this UAV. Pixhawk is a high-performance, all-in-one control system that allows a drone to maneuver agilely [35]. In addition, it has open-source hardware and software, enabling us to modify the software to accommodate the gasoline engines of the drone. Figure 2 shows the prototype with the two gas engines installed on the Y-axis of the drone frame to distribute their weights, and four electric motors placed as the quadcopter. Each gasoline engine weighs 0.96 pounds, and the entire gas system, including fuel tanks, mounts, and driving components, weighs 4.65 pounds. The fundamental drone components, including the frame and electrical system, weighs 5.33 pounds. In total, the hybrid drone weighs 9.98 pounds.

Despite the 87% increase in weight from the addition of the gasoline system, thoughtful operation of the hybrid propulsion system can significantly increase the drone’s flight time. The gas engines operate on a constant thrust to provide the majority of the lifting force. Hence, the electric motors provide stability and maneuverability, as they have a faster response time. The gas engines and electric motors independently produce thrust, so in Section 5 we identify the optimal thrust ratio between the two propulsion systems.



**Figure 2.** Hybrid hexacopter top and side views.

#### 3.1. Electric Propulsion System

The electric propulsion system consists of four brushless Swellpro 3508 650 kv DC motors with DJI carbon fiber  $12 \times 4.2$  propellers, which comply with the recommendations by the Tarot 680 distributor. These motors primarily control the drone’s stability and maneuverability, and they produce partial thrust. A main 4 s 7500 mAh LiPo battery is used to power these motors through four electronic speed controllers (ESCs) designed to invert the DC power to a three-phase source to control the motors. Figure 3 illustrates the wiring diagram between the electrical components on the prototype. The main battery also powers the flight controllers and the primary electronic devices. A secondary, lower voltage battery powers the gas system’s electrical components such as servos, spark plugs, and engine safety failsafe.

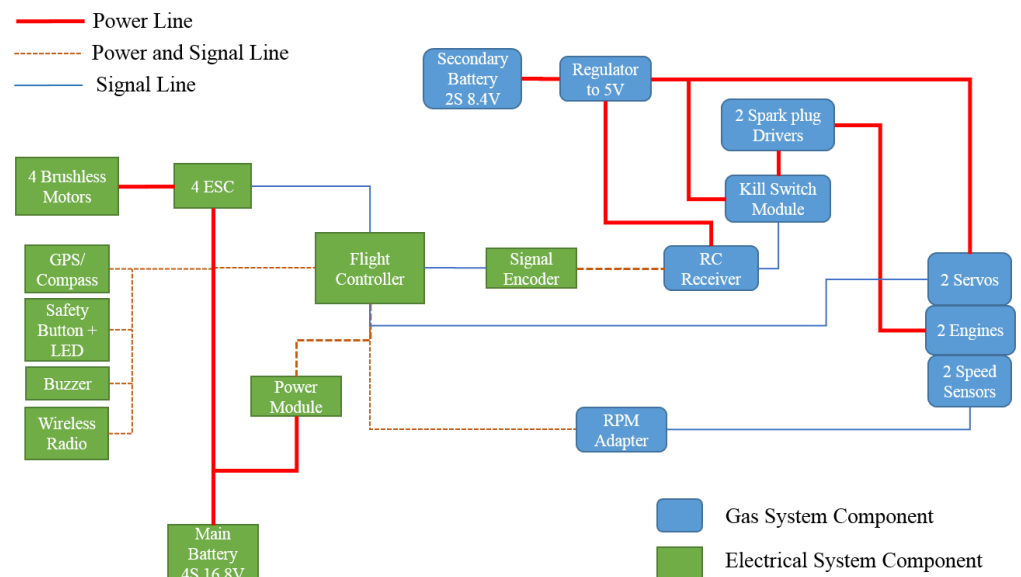


**Figure 3.** Electrical diagram showing the connections between the electric and gas system components.

Several procedures have been taken on this prototype to protect it from electromagnetic interference (EMI). EMI may arise due to the high current running through the power lines, which can heavily disturb the signal lines, particularly the magnetometer sensor reading, which is essential to determine the yaw heading of the drone. Therefore, a separation between signal and power lines was implemented as often as possible to mitigate the EMI disturbances. Furthermore, the magnetometer sensor was installed 17.5 cm above the drone platform, as shown in Figure 2.

### 3.2. Gas Propulsion System

The two EVO10GX2 gas engines provide most of the lift force for the drone. This engine is a 10 cc single-cylinder 2-stroke engine. It is relatively small in size and light in weight to fit into the tight space of the drone [36]. The gasoline engines come with an ignition module, ignition sensor, spark plug, and a high-resolution Hall-effect sensor, which determines the spark plug firing time and provides an accurate reading for the engine's revolutions per minute (RPM). Setting the RPM occurs by controlling the air intake on the carburetor through a servo attached to a single rod.

The fuel for this engine requires a mix of 20:1 gas to oil, and 87 octane is suitable for this engine. Each gasoline engine came with an 8 oz fuel tank from Evolution Engines. The manufacturer also produces solutions to avoid the fuel bubbles problem. The fuel bubbles may cause quivers, sporadic instability in the gasoline engine, and maybe a shutdown [34]. EVO10GX2 comes with a felt filter clunk used in the fuel tank to stop the air bubbles from reaching the carburetor via the fuel delivery pipes. This filter is pivotal and is designed to give a reliable flight for the hybrid drone.

Installing the two gas engines on the opposite sides of an electric quadcopter requires that their propellers' rotation directions are opposite to each other. One is clockwise, and the other is counterclockwise to cancel the torque and minimize the yaw correction provided by the motors. One difficulty we faced with these gas engines was the rotation direction. As manufactured, these gas engines rotate only in the counterclockwise route. Therefore, we manufactured a new crankshaft to reverse the rotation direction of one gasoline engine. We replicated the original crankshaft design but repositioned the air intake hole to the mirrored location of the original crankshaft. The engine successfully rotates in the clockwise direction after reallocating the Hall-effect sensor for proper ignition timing.

The gasoline engine's fuel flow was tuned manually by adjusting the low-speed and high-speed needles. Therefore, under the same conditions, each engine performs somewhat differently. However, the modified engine also showed less fuel efficiency due to the imperfect replication of the crankshaft and the difficulty of replicating the exact size of the air intake hole. Table 1 shows the fuel consumption rates for both gas engines. The engines were tested outdoors with identical Gefman 11 × 4.5 plastic propellers, discussed below.

**Table 1.** Gas engine's fuel consumption rates.

RPM	Reversed Crankshaft Engine Fuel Consumption (mL/min)	Normal Crankshaft Engine Fuel Consumption (mL/min)
6000	1.99	2.3
8000	4.11	3.19
10,000	5.84	5.18

Selecting the appropriate propellers puts less stress on the engines and economizes fuel consumption. As the recommended propellers are designed only for counterclockwise rotation, we chose new propellers due to the modification applied to one gasoline engine to rotate within the clockwise course. The recommended propeller for these engines ranges from 10 × 6 to 13 × 8 [36], and they use propellers designed for electric motors. A Gefman 11 × 4.5 plastic propeller was selected as it has a low pitch value with less turbulence, thus providing more stability for the drone, less fuel consumption, and increasing flight time [37]. Furthermore, it has an appropriate size that will provide the lift needed for the drone without consuming much fuel. The 11 × 4.5 electrical plastic propeller performed similarly to the 12 × 6 electrical carbon propeller, but it is more durable. The material used in the propeller's construction may affect its efficiency at various RPMs. Figure 4 shows an experimental test for different propellers and shows that the 11 × 4.5 plastic propeller originally manufactured for electrical motors was suitable for the gas engine. Note that 12 × 3.8 has better thrust than 11 × 4.5, but it consumes more fuel as it sweeps more air and responds slower to the input.

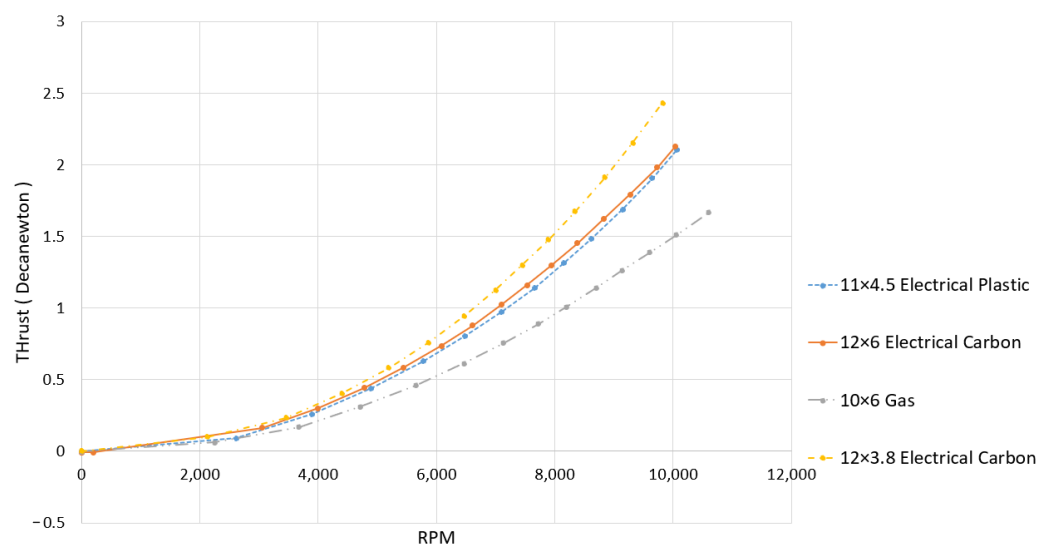


**Figure 4.** Thrust output of various propellers for the range of engine RPM values.

Because the engines are not intended for implementation on a drone frame, placing them on the drone's y-axis necessitated a novel mount design. The mount needs to connect to the drone's cylindrical arm and have flat surfaces to mount the engine and carburetor-controlling servo. Two design iterations are shown in Figure 5. Initially, an aluminum mount was designed for robustness. Holes were drilled out to reduce its weight, but each mount still weighed 0.22 pounds. A lightweight and easy-to-manufacture alternative used ABS plastic, which was 3D printed into a mount. This is significantly lighter in weight, but ABS plastic has a lower Young's modulus than aluminum, thus making it more susceptible to fracture. Young's modulus, which is essentially the material's stiffness, is crucial to be considered with this mount [38]. After performing finite element analysis to locate the weakest spot, a flange was attached to this mount to reinforce it. The final mount, made of ABS plastic, weighs 0.10 pounds. Hence, this mount is light in weight and less susceptible to fractures.

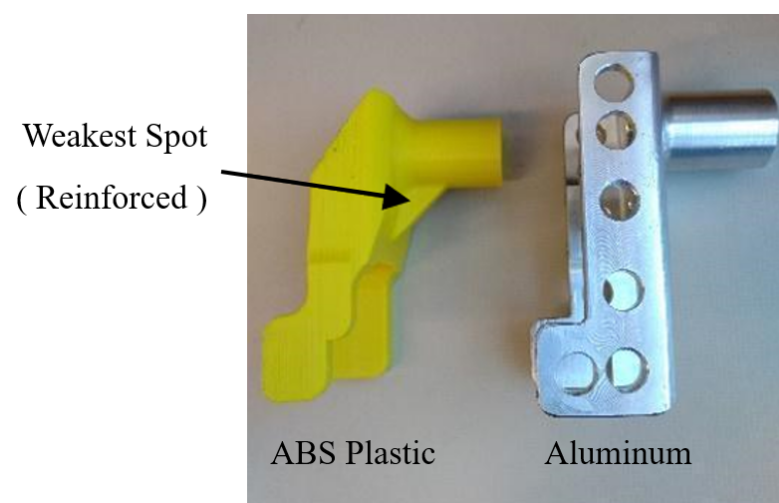


**Figure 5.** Two gasoline engine mount designs. The mount made of ABS plastic was lighter in weight but weaker, so was reinforced. The mount made of ABS plastic was implemented onto the prototype.

Even though gas engines can lead to increased flight time, the gas engine's vibrations can severely affect the drone's performance. These vibrations could dramatically affect flight stability, break the engines apart at high RPMs, and damage the frame structure [39]. Rubber mount shock absorbers with bolts extending from both sides of a rubber center were placed between the gas engine and its mount to mitigate these vibrations. These absorbers are light in weight and have a large elasticity which can effectively protect the structure. Various shock absorbers are available, including spring dampers, wire rope isolators, and air isolators. As a result, the shock-absorbing system might be developed further to assure structure longevity.

The flight controller, Pixhawk, is responsible for providing reliable flight stabilization. To ensure a stable flight, the vibrations read by the accelerometer sensor should not rise above/below  $\pm 3 \text{ m/s}^2$ , which confirms that the shock absorbers are necessary for drone stabilization. Figure 6 plots the vibrations along the drone's x-axis when the engines run for a while. As shown in Figure 6, the pulses are excessive before lifting off the ground, caused by the collision between the drone's frame and the floor. However, the vibration experiences a dramatic reduction when leaving the ground and stays within limits.

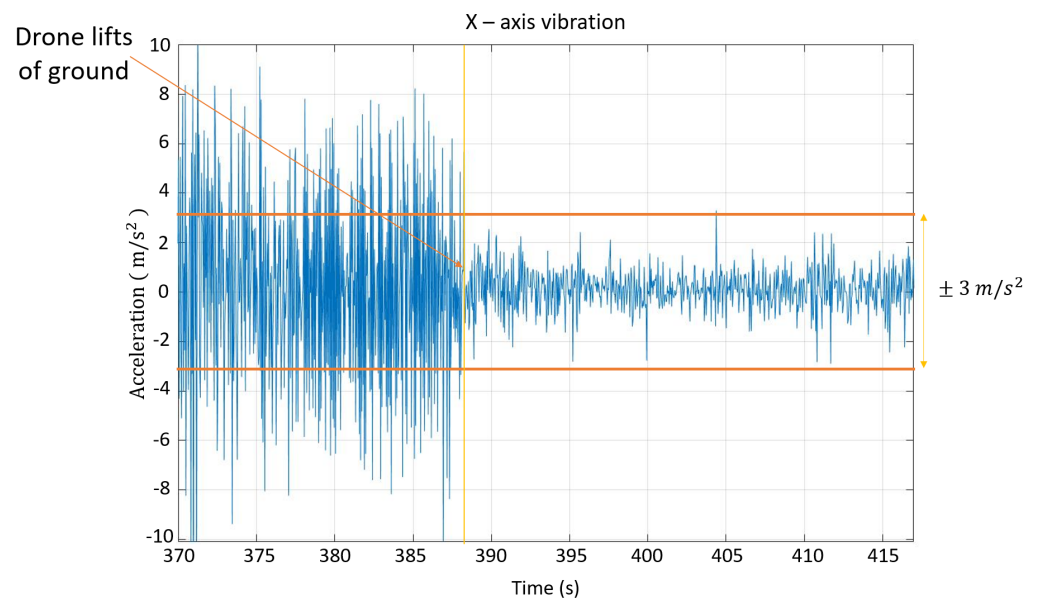


**Figure 6.** X-axis engine vibrations. When the drone lifts off the ground, the vibrations reduce to be within the acceptable range for the flight controller.

### 3.3. Controller Modifications

The primary electronic device on the prototype is the flight controller, Pixhawk. It is a high-performance autopilot device provided with an ARM Cortex-M4 processor running at 168 MHz, executing advanced control algorithms [40]. Due to the Pixhawk being open source for both hardware and software, it was suitable for the prototype, as modifying the software is necessary to incorporate the two gas engines.

The essential role of the gas propulsion system is to provide the lift force for the prototype. It is also necessary that the two gas engines rotate opposite each other to minimize the yaw correction provided by the motors. The engines received the desired RPM from the user input. However, the RPM for both engines will not be identical because each gasoline engine was manually tuned. Hence, two PI loop functions were added to Pixhawk's software v1.8.2 to control the engines' RPM.

The prototype's Pixhawk was configured for a quadcopter, thus providing the automatic stabilizing feature for the electric propulsion system. The two PI loop functions receive the RPM feedback readings from the Hall-effect sensors and adjust the servos that control the throttle opening of the engine. Several experimental tests were conducted to tune the performance of these PI functions and achieve a  $\pm 200$  RPM error margin, which is shown in Figure 7. The derivative gain was not used because the inertia of the gas engines rendered D largely ineffective in providing stability. Note that in Figure 7 the response time for the gas engines to go from around 4400 RPM to 8000 RPM is approximately 3 s. However, this is not a primary concern as the gas propulsion system is intended to provide constant thrust during the flight.

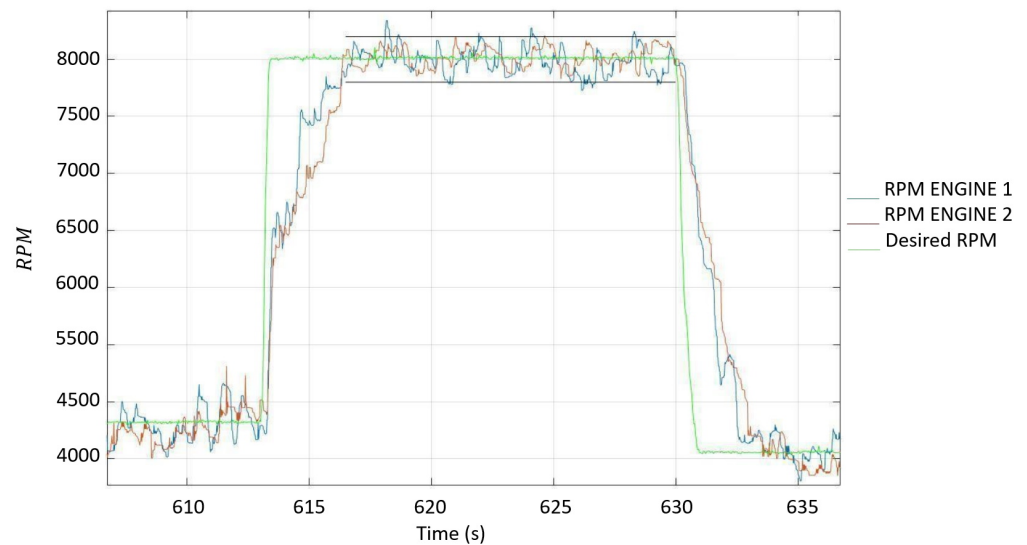


Figure 7. Gasoline engine RPM controller test.

#### 4. Characterization of Propulsion Subsystems

As the prototype's hybrid propulsion system targets increasing the flight time, each propulsion system was characterized to understand how its thrust output relates to its energy consumption. These relationships were directly applied to the propulsion system model in Section 6 to determine the exact amount of energy reserves necessitated to achieve the maximum flight time. The prototype aims to consume all the fuel in tanks and the battery in flight, not to carry unnecessary weight.

##### 4.1. Electric Propulsion System Characterization

The primary role of the motors is stabilizing the prototype. Even if there is fuel in the engines to provide the lift, the prototype cannot hover without stabilization. Thus, the electric propulsion system was investigated to determine how the thrust is related to the current drawn. Hence, finding the optimal thrust required from the motors to have a stable flight is necessary. Going below this thrust will affect the motor's efficiency to stabilize the drone, thus no stable flight. On the other hand, going above this thrust will draw more current and reduce flight time. The system model in Section 6 will use this relationship between thrust produced and current drawn to determine the drone's maximum flight time.

One brushless DC motor and propeller were investigated to find the relationship between the current consumption and the thrust. The electric propulsion system consists of four electric motors, and the output will be multiplied by four to represent the entire electric propulsion system. Several tests were conducted on an RC Benchmark Series 1580 thrust stand and dynamometer. It is equipped with an optical sensor to measure the RPM and a strain gauge load cell to measure thrust and torques applied from the motor. This thrust stand can measure up to 11 lbf of thrust and 1.5 Nm of torque [41]. It was connected to a laptop via USB to run its software, which automated the testing process and logged all sensor measurements. Figure 8 shows the characterization test setup.

The test was conducted by supplying the motor with a current ranging from 0 A to 13 A back and forth. The current range was covered twice, and the input steps were given a settling time before changing to reveal the hysteresis error in the system and sensors. Figure 9 shows the thrust produced by the motor at various current consumption rates, and as shown, the hysteresis error was minimal as the ascending and descending curves are nearly identical. The system model uses this relationship to determine the optimal thrust necessary from the motors to stabilize the drone.

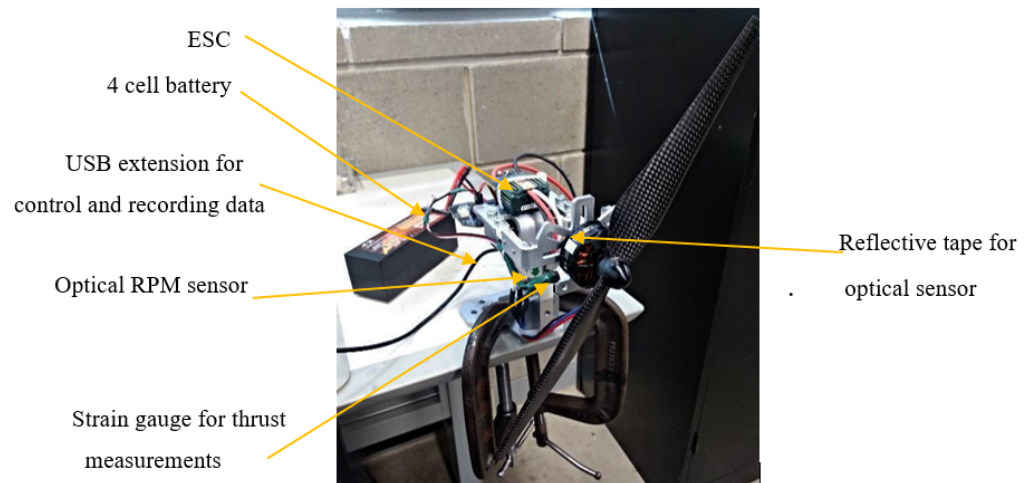


**Figure 8.** Brushless motor characterization test setup.

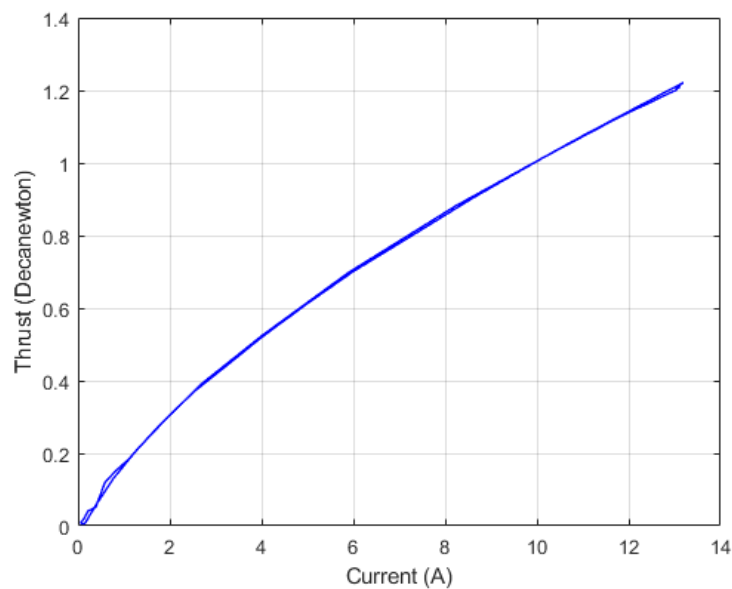


**Figure 9.** Thrust output of the electric motor and propeller across various current consumption rates.

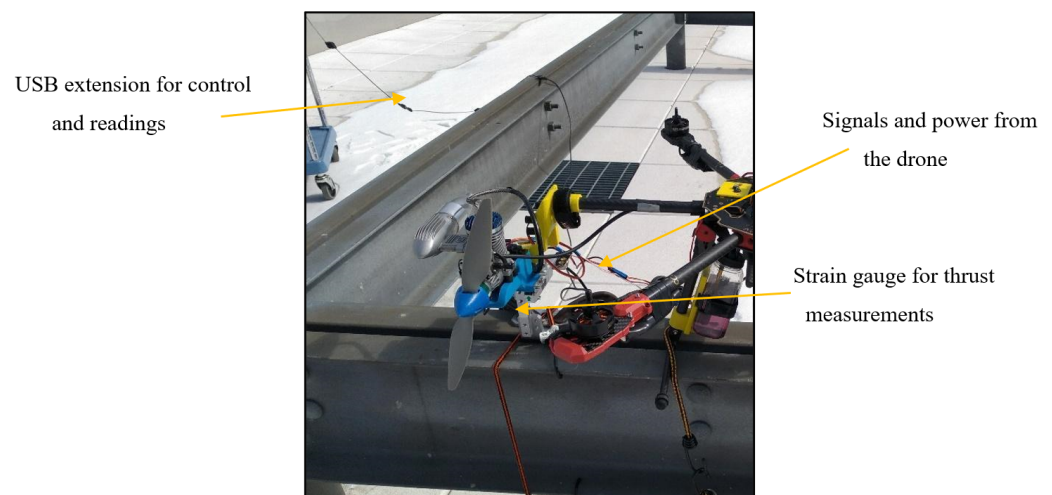
One important consideration when conducting the test is the battery voltage. A 4 s 7500 mAh LIPO battery voltage varies from 16.8 V fully charged to 14 V when it is empty. This variation significantly affects the relationship between the thrust produced and the current, as the thrust decreases when the battery voltage drops. The calculated average battery voltage for the tests was 15.34 V. The 15.34 V was selected to conduct the simulation test in the system model.

#### 4.2. Gasoline Propulsion System Characterization

As mentioned before, the primary function of the two gas engines is to provide the majority of the lift force to the prototype. However, the amount of fuel in the tanks and the thrust required from the gas engines considerably affect the flight time. The relationship between the thrust and the fuel consumption was characterized to determine the optimal thrust required from the gasoline engines. This relationship significantly determines the fuel amount the prototype should have until consuming all the energy reserves during the flight.

First, the two gas engines were characterized to obtain the relationship between the thrust and the fuel consumption. However, as shown in Table 1, there is a slight difference between the two gas engines. The modified clockwise engine has lower fuel efficiency than the unmodified one as it is equipped with a customized crankshaft. Furthermore, gas engines are complex. Their performance may be affected by several factors such as the ambient temperature, humidity, engine tuning, and the variety of the internal engine temperature upon increasing or decreasing the RPM, which add difficulties in matching the fuel consumption between these two engines. Therefore, the unmodified engine was chosen to be characterized for modeling purposes in Section 6. Multiplying the outputs by two represents the entire gasoline propulsion system.

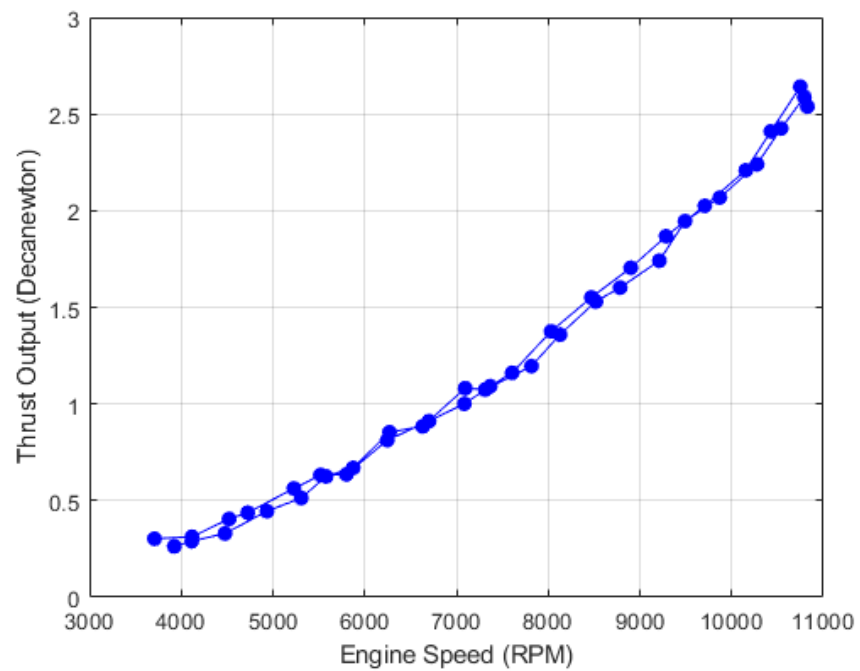
This characterization process involves the flight controller since the PI loop function controls keep the gas engine running at the desired input RPM. The RPM was selected to be an intermediate variable. Thus, two tests were conducted to obtain how the thrust and the fuel consumption are related. Figure 10 shows the first test setup connecting the output thrust with the RPM, which utilized the same RC Benchmark Series 1580 as in the electric characterizations. An auxiliary mounting part with shock absorbers was installed to attach the engine to the main structure and eliminate the vibrations produced by the engine. The RC benchmark software automated the test, which commanded the Pixhawk to control the gas engine RPM speed. The RPM was divided into steps and varied from 4000 RPM to 10,000 RPM back and forth, which involved approaching the entire range twice to reveal the hysteresis error in the system.



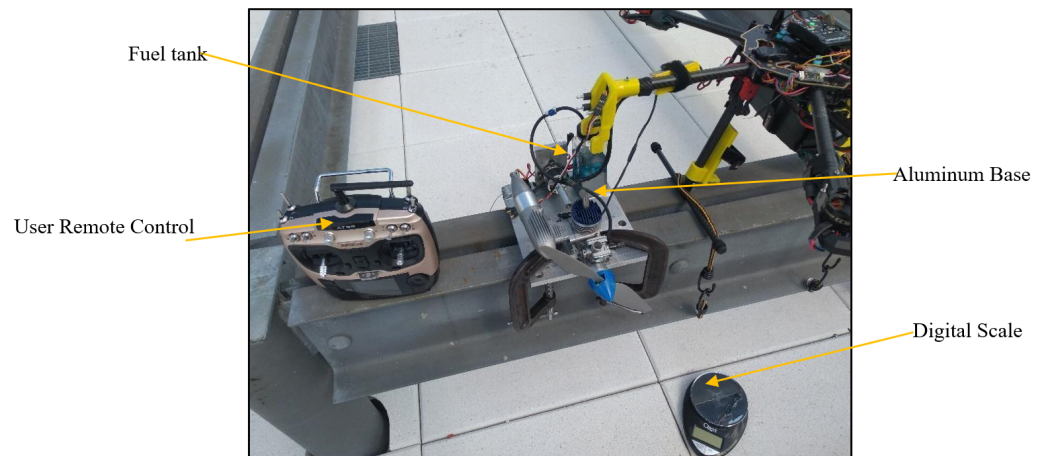
**Figure 10.** Gasoline engine test setup (thrust vs. RPM).

Figure 11 shows the relationship between the thrust and the RPM. Note that the hysteresis error is obvious and considerable. This difference is attributed to the vibration produced by the engine and the potential energy stored in the shock absorbers of the engine's mount.

The second characterization test was conducted to obtain a relationship between the RPM and fuel consumption rates. Figure 12 shows the test setup in which the engine was fixed to a stationary test bench and was connected to the Pixhawk to receive the speed commands. Eight speeds were received manually from the user input control between 4000 RPM to 11,000 RPM, maintaining every speed for ten minutes. The fuel tank was weighed before and after each test by a digital scale with one gram of precision. Thus, the fuel consumption rate was calculated as shown in Figure 13.



**Figure 11.** Thrust produced by a single engine at various speeds.



**Figure 12.** Gasoline engine test setup (RPM vs. fuel consumption rates).

The relationship between the thrust and the fuel consumption rates was obtained from the two characterization tests shown in Figures 11 and 13. As the RPM was controlled via the PI control loop, it was the intermediate variable between them. Hence, the two equations obtained from these figures will be applied to the system model in Section 6 to maximize the prototype's flight performance.

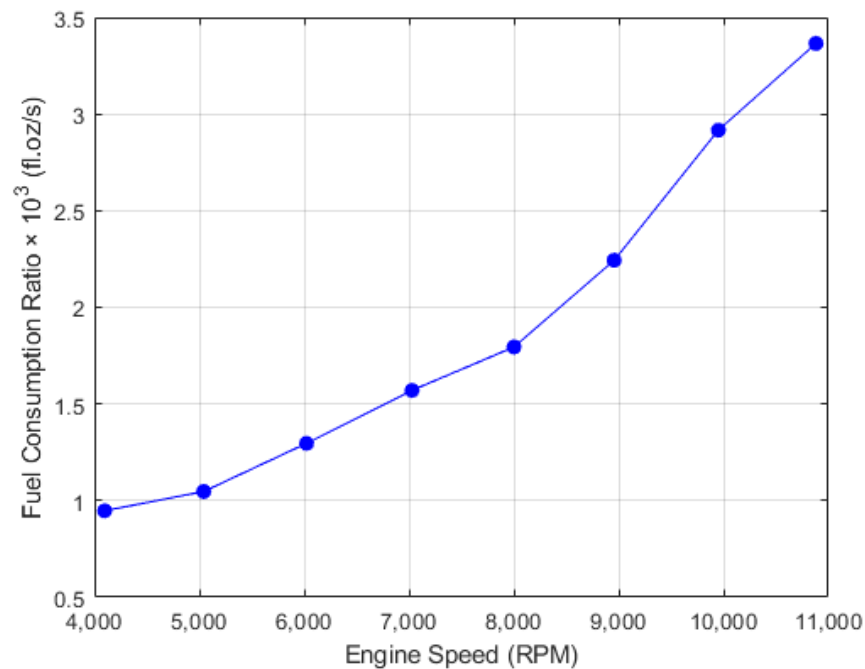


**Figure 13.** Fuel consumption rate of a single engine at various speeds.

### 5. Gas/Electric Ratio Optimization

One of the most significant factors affecting the hybrid prototype's flight time is the thrust required from each propulsion system. The gas-to-electric thrust ratio is a parameter that expresses the thrust output required from each propulsion system. For example, a 75:25 thrust ratio means the gasoline propulsion system produces 75% of the total thrust force, and the electric propulsion system produces the remaining 25%. Operating at any given thrust ratio affects the rate of fuel and the battery capacity consumed.

Since the prototype should achieve maximum flight endurance, the motors should consume enough current to stabilize the drone and fly agilely. Due to the prototype's significant moment of inertia (MOI), as it is equipped with two gasoline engines, the torque needed to rotate the drone and recover from any disturbance is high; thus, more current is required for the motor to stabilize the drone. As a result, the thrust produced by the gasoline propulsion system was experimentally selected by determining the minimal amount of current required for the electric motors to stabilize the drone effectively.

Several simulations and experiments were conducted to find the optimal thrust ratio. Furthermore, this ratio determined the amount of fuel in each tank. Filling the tanks with extra fuel decreases flight time and consumes more current from the battery as the drone's weight increases. Hence, filling the tanks with the exact amount of fuel makes the prototype deplete all the energy reserves simultaneously and achieve maximum flight time.

### 6. System Modeling

The mathematical model of the prototype was simulated and analyzed utilizing MATLAB Simulink. The model investigated how the weight and energy density of the gasoline and battery carried onboard affected the prototype's flight time for different gas-to-electric thrust ratios. Adding further energy reserves requires more thrust from each propulsion system to produce the necessitated lifting force and stabilization. The simulation showed that maximum flight time is achieved when the drone operates at a high gas-to-electric thrust ratio and all the energy reserves are depleted simultaneously.

### 6.1. Model Development

Mathematical model simulation can efficiently predict the prototype behavior without extensive testing. Figure 14 shows the model that examines the relationship between thrust output, energy consumption rates, and the varying prototype's weight throughout the flight. Battery capacity, fuel volume, and gas-to-electric thrust ratio are the model's inputs, with the flying time being the output. For simplicity, the only operating scenario considered was hovering in ideal conditions with no external disturbances, so the model neglects the drone's responsive behavior and physical dimensions.

The required thrust from each subsystem is determined by the weight of the drone and the gas-to-electric thrust ratio. If the required thrust exceeds the motor thrust limit, a stop signal is generated. In other words, if the simulation inputs of fuel weight and battery capacity exceed the maximum weight that the motors/engines can lift, the simulation will be terminated.

If the inputs will allow the prototype to fly, the next relevant blocks are the gasoline system, electric system, and drone weight calculation blocks. The gasoline and electric system blocks employ the equations derived by the characterization processes for each actuator to calculate the energy reserves needed when a specific thrust force is required. Third-degree polynomial functions were fitted for this purpose using the MATLAB curve fitting toolbox. The simulation multiplies the performance of a single electric motor by four when calculating the amount of energy required, which is consistent with the ideal hovering assumption. Furthermore, the model assumes that the battery voltage stays at 15.34 V for the entire simulation run, which is the same voltage used in the motor characterization test. In the gasoline system block, both gas engines are assumed to perform according to the unmodified engine. This decision was made to demonstrate the potential of the prototype in the case where engines are commercially manufactured in both clockwise and counterclockwise rotation directions.

The drone weight calculation block is crucial in the simulation because multirotor drones must actively overcome their weight. It is shown in detail in Figure 15. The initial weight is calculated from the fuel amount, battery capacity, and fuel tank size while keeping all other fixed weights. The battery mass depends on cell count, cell configuration, and cell capacities and is calculated using the following equation [42]:

$$m_b = (P_1 + s + P_2) * c \quad (1)$$

where  $c$  is the battery capacity,  $s$  is the battery cell count,  $P_1$  is 0.026373, and  $P_2$  is  $2.0499 \times 10^{-5}$ . The weight of the fuel tank was estimated using a proper function based on vendor specifications [43]. Note that in Figure 15, the only variable that changes the drone's weight while the model is running is the weight of fuel consumed. As the prototype consumes fuel, its weight decreases, so the drone weight calculation block iteratively calculates the prototype's weight. This decrease in weight results in less thrust required to lift the prototype, thus prolonging flight time.

The weight limits block after the drone weight calculation block determines whether or not the required thrust from each motor engine can be achieved. This is important for determining whether the inputted battery and fuel amounts are feasible for hovering.

The final block in the simulation compares the energy consumption to the remaining fuel and battery capacity. The simulation terminates the flight when the prototype entirely consumes the battery. The prototype can fly in two modes, either hybrid or fully electric. Therefore, the simulation also ends if there is still energy in the battery, but the fuel is depleted and the electric motors' total thrust is insufficient to lift the prototype.



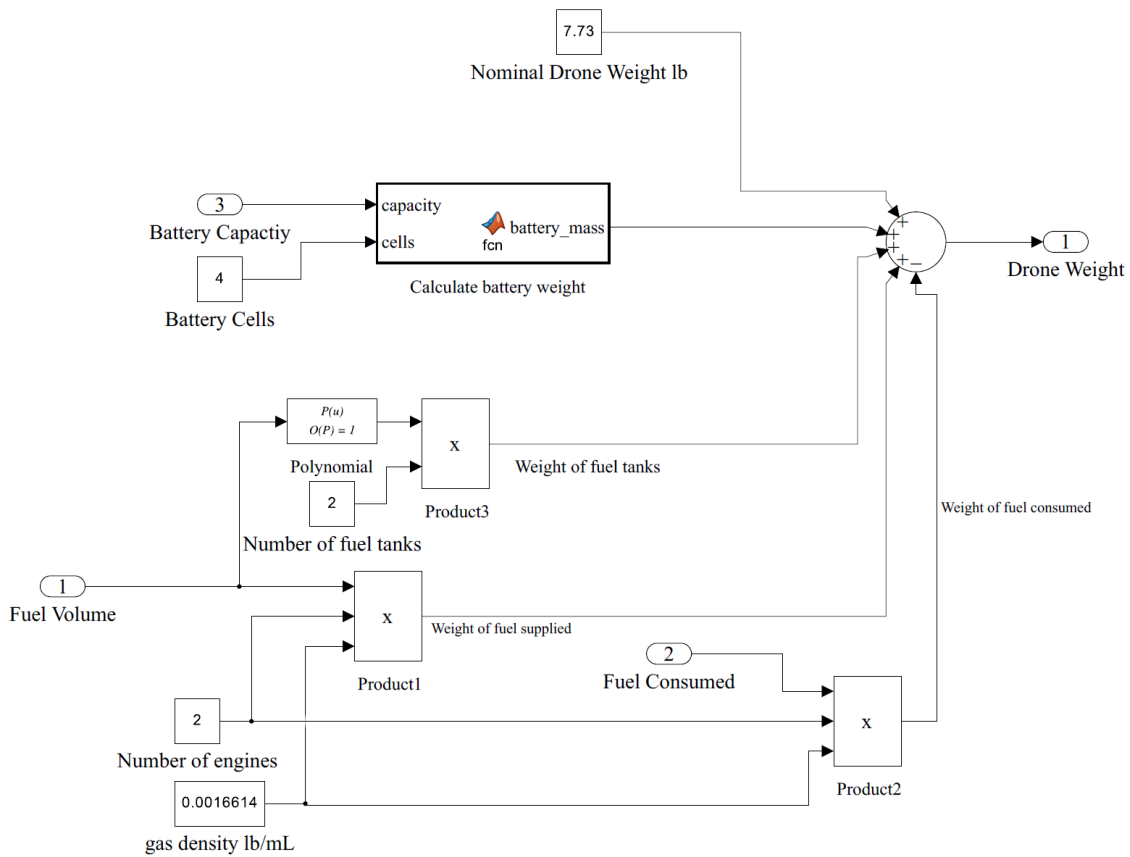


Figure 15. Drone weight calculation.

6.2. Simulation Results

The hybrid gasoline–electric hexacopter performance was evaluated by conducting extensive simulations. Figure 16 shows the fully electric flight simulation while the gasoline propulsion system is off. This result indicates that the maximum battery capacity the prototype can carry is 13 Ah. Thereafter, more thrust is required to overcome the drone’s weight, which the electric motors cannot provide.

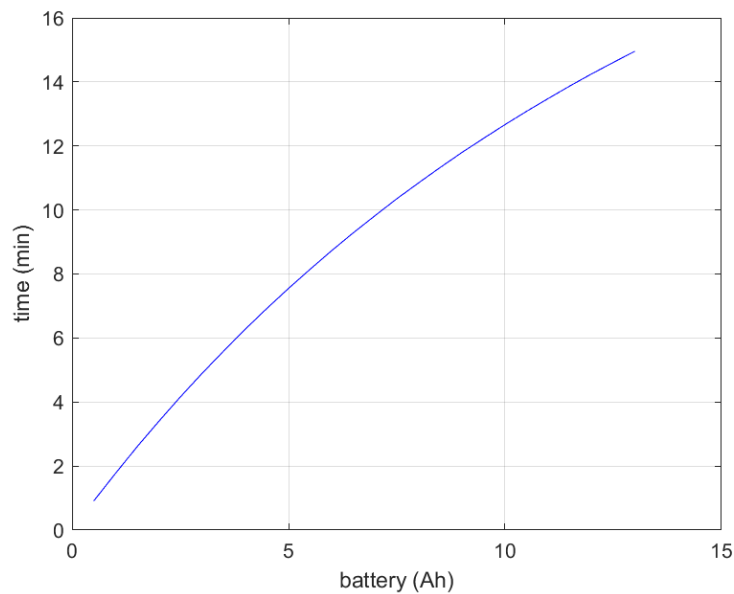
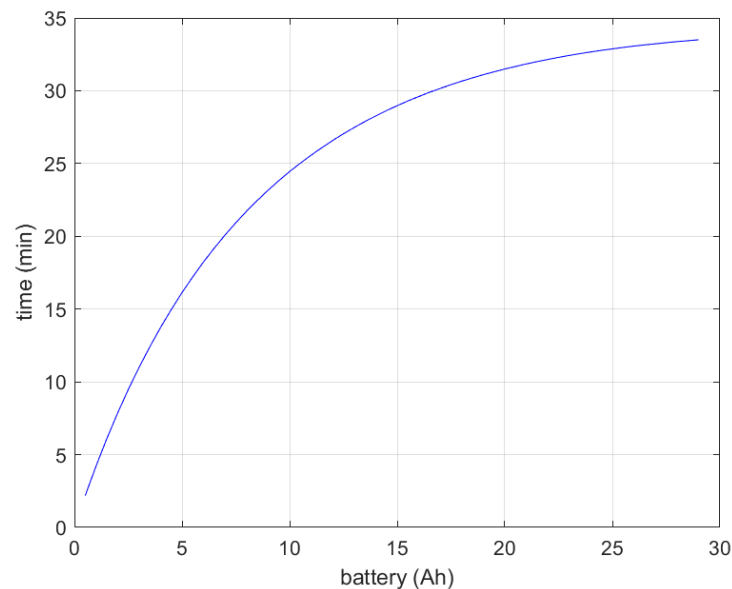


Figure 16. Electric-only flight time, including gas components.

Figure 17 shows the fully electric flight simulation when the gasoline system is excluded from the drone. This decreases the drone's weight by 5.33 pounds and has a maximum flight time of 33 min. This figure aims to show the flight time improvement achieved by adding the gasoline propulsion system.



**Figure 17.** Electric-only flight time, excluding gas components.

One crucial function of the simulation is determining the proper weight of fuel and battery capacity for a specific gas-to-electric thrust ratio. This ensures no extra weight is carried onboard and results in maximum flight time. Figure 18 illustrates the flight time for a range of fuel volumes and battery capacities with a 50:50 gas-to-electric thrust ratio. Note that there is an optimal line that bends the 3D plot into a pyramid shape. This line shows fuel and battery capacities that are depleted simultaneously, which provides optimal fuel and battery capacity estimates to carry onboard the drone. Using these points on this line facilitates the hybrid electric and gas propulsion systems design for drones with the same components and configuration as the introduced prototype.

The region to the right of the optimal line in Figure 18 shows the points at which the battery drained first. Meanwhile, the left part represents the points when fuel is exhausted first. An empty fuel tank forces the prototype to switch to a fully electric operation. However, the total thrust generated by the electric motor is insufficient to lift the prototype when the battery is above 13 Ah, as previously shown in Figure 16. This case is clearly shown in Figure 18 as there is a step down to lower flight times after switching to the fully electric operation with a 13 Ah battery or higher. The 50:50 ratio achieves a simulated flight time of 26 min with a 7500 mAh 4-cell LiPo battery and 90 mL of fuel. This short flight time is because the 50:50 gas-to-electric ratio is insufficient to utilize the gasoline propulsion system. Furthermore, adding more gasoline fuel at this rate will increase the prototype's weight, reduce flight time, increase pressure on the electrical system to stabilize the drone, and drain the battery faster.

Increasing the thrust required from the gasoline engines is necessary to utilize the gasoline propulsion system further. This increase allows the gasoline engines to provide more lift to the prototype and reduces the current drawn by the electric motors. Figure 19 shows the flight times after increasing the gas-to-electric thrust ratio to 75:25. This ratio achieves a simulated flight time of 60 min with a 7500 mAh 4-cell battery and 480 mL of fuel, 240 mL in each tank, which equals the prototype's fuel tank size. As a result, this ratio achieved nearly triple the drone's flight time with no gas propulsion system, as shown previously in Figure 17. Following the optimal line provides a reasonable estimate of the required energy reserves. Replacing the battery with a 15,000 mAh LiPo battery

and increasing the fuel tanks size to accommodate 470 mL of fuel, 940 in total, caused the simulated flight time to rise to nearly 98 min instead of 28 min achieved with the electric-only flight time.

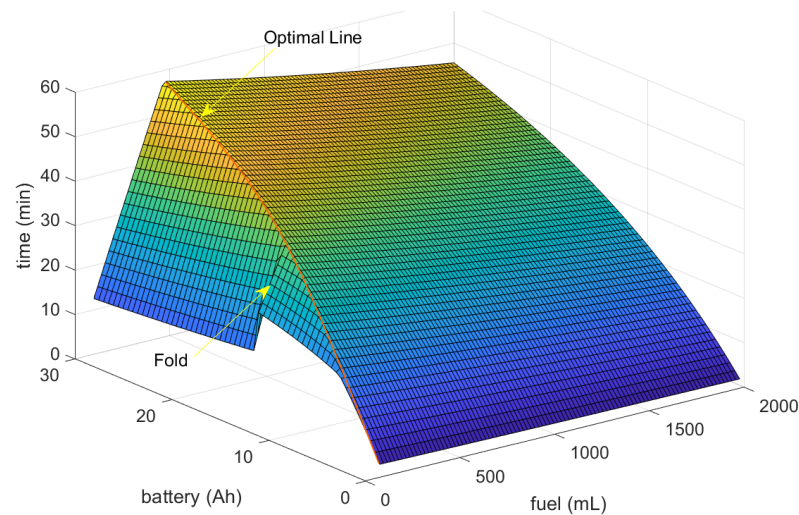


**Figure 18.** Flight times for 50:50 gas-to-electric ratio.

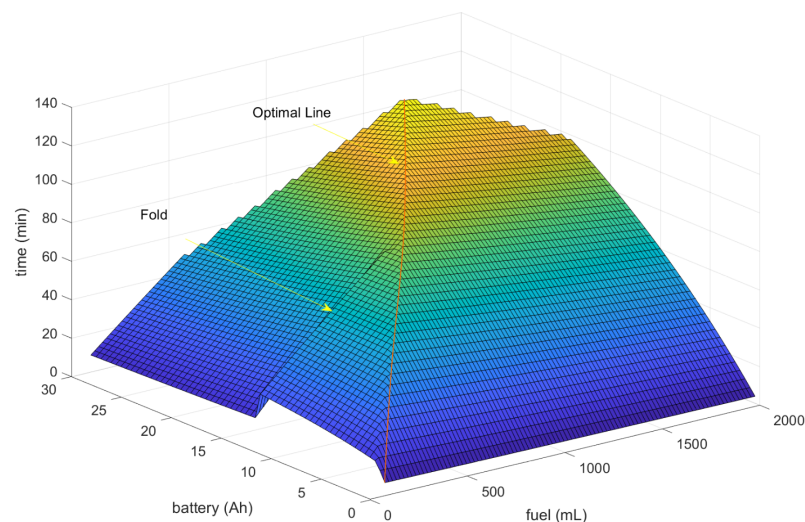


**Figure 19.** Flight times for 75:25 gas-to-electric ratio.

The simulation also determines the optimal gas-to-electric thrust ratio for a given battery capacity and fuel tank size. The prototype is equipped with a 7500 mAh LiPo battery and two 8-ounce, 240 mL fuel tanks. Figure 20 shows the flight times using a 7500 mAh LiPo battery with varying fuel volumes and thrust ratios. It also shows the optimum gas-to-electric thrust ratio for the prototype, which is found at 75:25 for this particular battery capacity. A distinct line that divides the plot into two parts represents the optimal gas-to-electric thrust ratios for the 7500 mAh battery with different fuel amounts. The left side of this optimal line shows that as the gas-to-electric thrust ratio increases, fuel is consumed before the battery is depleted. Hence, a reduction in the flight times occurs as the prototype switches to function fully electrically, causing battery drain. Note that the prototype MOI is high due to the presence of the gas propulsion components. Experiments show that increasing this ratio beyond 80:20 will impair the stability of the drone. Reducing the electric thrust below 20% will slow down the angular recovery rate when stabilizing the drone and affect maneuverability performance.

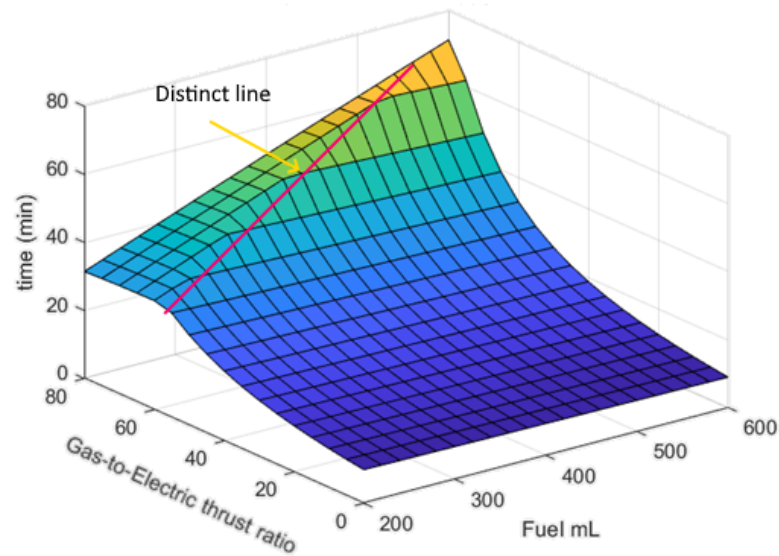


**Figure 20.** The flight time for a fixed 7500 mAh LiPo battery.

## 7. Experimental Evaluation and Conclusions

Several experiments were performed to evaluate the effect of the gasoline system on the prototype's flight time. These included restrained tests that forced the prototype to hover ideally and free flight tests where the prototype was faced with true-to-life conditions. Furthermore, experiments were compared to the simulation results to assess the validity of the model and predict the drone's flight time in ideal conditions.

Figure 21 shows the components used when testing the drone in ideal hovering conditions. The test stand restricts roll, pitch, and yaw movements to mimic the hovering conditions in the simulation, and the drone is directly coupled to a strain gauge to measure its pulling force, which corresponds to the lift force produced by the drone. When the lifting force on the strain gauge incrementally exceeded the drone's weight, the drone was considered to be hovering. The Pixhawk collects the overall current consumption of the electrical components and RPMs for the gasoline engines. Since one of the gasoline engines has a modified crankshaft, which reduces its efficiency, the data analysis only considered the unmodified gasoline engine's fuel tank. This is consistent with the assumption made in the simulation model and serves to predict the behavior of the prototype in the ideal case where engines are available in both rotational directions.



**Figure 21.** Equipment used in controlled experimental testing. The test stand enforced ideal hovering conditions.

To operate at a specific thrust ratio, the gas engines' speed and the current drawn by the electric motors were determined from the simulation's calculations. The test began with the startup of all actuators at a low speed. The RPM of the gasoline engine was increased via the remote control to reach the required RPM. Then the electric motors' speed was increased and tuned until the total current measurement matched the current requirement specified in the simulation. The strain gauge measurement verified that the prototype was "hovering". Timing began when the gasoline engines started and continued until one or both energy reserves were completely depleted. The recorded time represented the flight time of the drone.

Figure 22 shows how four experimental tests compare the simulation model at various gas-to-electric thrust ratios. All tests were conducted with a 7500 mAh battery, a full 8-ounce fuel tank on the unmodified engine, and an external fuel tank on the modified engine. As expected, long flight times were achieved with high values for the gas-to-electric thrust ratio. As the gas-to-electric thrust ratio was increased, the current draw on the motors decreased while dependence on the gasoline system increased. Because gasoline has a higher energy density, the prototype was able to operate longer when it derived more of its lift from the gasoline system, resulting in significant flight times. A total of 50 min of operation was achieved on the test stand with a 75:25 gas-to-electric thrust ratio, which was determined to be the optimal gas-to-electric thrust ratio. This flight time is a significant improvement upon battery-only flight times and shows that hybridizing a multirotor drone with a gasoline system can increase flight time.

Note also that the actual flight times in Figure 22 almost consistently show lower values than the simulation results. While both the experiment and the model enforced conditions for hovering, there are several minor discrepancies between the two that likely aggregate into the observable difference in Figure 22. First, the assumptions in the simulation do not reflect how the voltage changed in the battery during operation. Next, weather conditions were not included in the model. Temperature and humidity affect the performance of the engines and thrust output of the propellers, which likely caused them to underperform in comparison to the characterization tests. Nevertheless, the matching trend between the simulated and experimental results shows that the model captured the basic behavior of the hybrid prototype. Thus, the suggestions made from the simulation in Section 6.2 can be used as a starting point for future gasoline–electric hybrid drone designs.

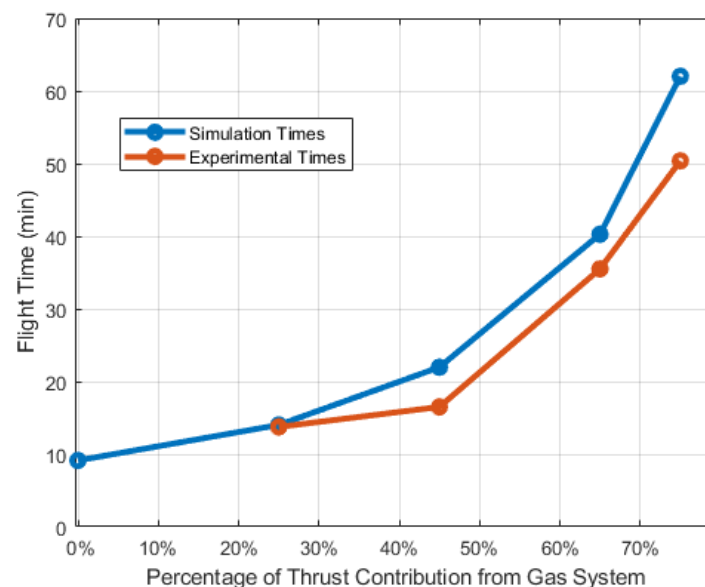


**Figure 22.** Comparison of simulated and experimental flight times. The experimental times were performed on a test stand to enforce ideal hovering conditions.

To compare the flight time of the prototype with conventional drones, Table 2 shows select fully-electric drones from different manufacturers. It is apparent that the hybrid gasoline–electric multirotor drone can outlast the other multirotor drones. More specifically, the hybrid prototype provides a 25% longer flight time when compared to one of the top-performing commercial drones, the DJI Matrice 100, which is equipped with two Intelligent Flight TB48D batteries [44]. The prototype in this study has a 44% higher weight than the DJI Matrice, which is due to the gas propulsion system’s parts, such as gas engines, fuel tanks, and drive components discussed in Section 3. While the commercial drone is likely at its peak flight time of 40 min, there is more opportunity to improve the prototype performance further, as discussed as future work in Section 8.

**Table 2.** Multirotor drones’ flight times.

Product	Flight Time (mins)	Total Weight (lbs)
xFold rigs TRAVEL X8 Octocopter [45]	up to 15	8.6
DJI Inspire 2 [46]	23–27	9.37
DJI Matrice 100 (Quadcopter with two TB48D battery) [44]	40	6.8
Professional UAV Thor X4 [47]	15	10
Prototype in this work	50	9.8

The prototype was also tested without a test stand. Figure 23 shows that the prototype successfully flew with a 75:25 gas-to-electric thrust ratio. While it could hover, careful control was consistently required from the pilot. Thus, the prototype was unable to sustain long flight times during free flight due to challenges with control. This was likely because the system was configured for ideal operation with no wind, and future work includes refining the control system to ease the strain on the pilot.



**Figure 23.** Experimental flight.

## 8. Summary and Future Work

A gasoline–electric hybrid multirotor drone was designed, modeled, tested, and analyzed to determine how the addition of a gasoline system affects the flight time of an electric multirotor drone. The hybrid prototype exploits the advantages of electric and gasoline propulsion systems to achieve a long flight time. The fast-response electric motors provide stability to the prototype, while the gasoline propulsion system provides the majority of the lift force. Operating the prototype with 75% of the lift coming from the

gas system and 25% of the lift coming from the electric system maximized its flight time, which was 50 min on a controlled test stand.

The simulation and the experimental results specified the optimal gas-to-electric thrust ratio, the fuel amount, and the battery capacity in which all the energy reserves were depleted simultaneously. This ratio can differ from one design to another based on the fuel tank size, battery capacity used, motors and engine types, and drone weight. However, each propulsion system should have sufficient thrust to execute its function fully.

With information from the optimal line, the proposed prototype can be reconfigured to enhance its flight performance and reduce energy consumption rates. Future work related to this study includes more detailed testing on engine performance, thrust distribution, and controller enhancement.

**Author Contributions:** All authors contributed equally to this work. All authors have read and agreed to the published version of the manuscript.

**Funding:** This research was funded by Michigan Space Grant Consortium grant number NNX15AJ20H, and National Science Foundation under grant number EEC-1659650.

**Institutional Review Board Statement:** Not applicable.

**Informed Consent Statement:** Not applicable.

**Data Availability Statement:** Data is contained within the article.

**Acknowledgments:** The authors would like to thank and acknowledge the contributions of undergraduate “REU” Student Dana Bigham for her contributions at the initial stages of the project. Peter Taylor and Derek Hurley, from the Oakland University SECS Machine Shop, are also gratefully acknowledged for their insights and skillful construction of the modified crankshaft for one of the gasoline engines. Finally, thank you to the funding agencies that supported different parts of this project.

**Conflicts of Interest:** The authors declare no conflict of interest.

## References

1. Wu, Q.; Zeng, Y.; Zhang, R. Joint trajectory and communication design for UAV-enabled multiple access. In Proceedings of the GLOBECOM 2017—2017 IEEE Global Communications Conference, Singapore, 4–8 December 2017; pp. 1–6.
2. Ustolin, F.; Taccani, R. Fuel cells for airborne usage: Energy storage comparison. *Int. J. Hydrogen Energy* **2018**, *43*, 11853–11861. [[CrossRef](#)]
3. Boukoberine, M.N.; Zia, M.F.; Benbouzid, M.; Zhou, Z.; Donato, T. Hybrid fuel cell powered drones energy management strategy improvement and hydrogen saving using real flight test data. *Energy Convers. Manag.* **2021**, *236*, 113987. [[CrossRef](#)]
4. Arat, H.T.; Sürer, M.G. Experimental investigation of fuel cell usage on an air Vehicle’s hybrid propulsion system. *Int. J. Hydrogen Energy* **2020**, *45*, 26370–26378. [[CrossRef](#)]
5. Sliwinski, J.; Gardi, A.; Marino, M.; Sabatini, R. Hybrid-electric propulsion integration in unmanned aircraft. *Energy* **2017**, *140*, 1407–1416. [[CrossRef](#)]
6. Townsend, A.; Martinson, C.; Gouws, R.; Bessarabov, D. Effect of supercapacitors on the operation of an air-cooled hydrogen fuel cell. *Heliyon* **2021**, *7*, e06569. [[CrossRef](#)] [[PubMed](#)]
7. Dudek, M.; Tomczyk, P.; Wygonik, P.; Korkosz, M.; Bogusz, P.; Lis, B. Hybrid fuel cell–battery system as a main power unit for small unmanned aerial vehicles (UAV). *Int. J. Electrochem. Sci.* **2013**, *8*, 8442–8463.
8. Aravindan, V.; Gnanaraj, J.; Lee, Y.S.; Madhavi, S. Insertion-type electrodes for nonaqueous Li-ion capacitors. *Chem. Rev.* **2014**, *114*, 11619–11635. [[CrossRef](#)]
9. Mecrow, B.C.; Bennett, J.W.; Jack, A.G.; Atkinson, D.J.; Freeman, A.J. Drive topologies for solar-powered aircraft. *IEEE Trans. Ind. Electron.* **2009**, *57*, 457–464. [[CrossRef](#)]
10. André, N. Design of Solar Powered Airplanes for Continuous Flight. Ph.D. Thesis, ETH Zürich, Zürich, Switzerland, 2018.
11. Riss, Š. Development of a Hybrid Power Unit for Unmanned Aerial Vehicles. Ph.D. Thesis, Czech Technical University, Prague, Czech Republic, 2017.
12. Bocarsly, A.B.; Niangar, E. Electrocatalyst Design for an Elevated Temperature Proton Exchange Membrane Direct Ethanol Fuel Cell. *ECS Trans.* **2008**, *16*, 1285. [[CrossRef](#)]
13. Kim, T.; Kwon, S. Design and development of a fuel cell-powered small unmanned aircraft. *Int. J. Hydrogen Energy* **2012**, *37*, 615–622. [[CrossRef](#)]

14. Rhoads, G.; Bradley, T.; Wagner, N.; Taylor, B.; Keen, D. Design and flight test results for a 24 hour fuel cell unmanned aerial vehicle. In Proceedings of the 8th Annual International Energy Conversion Engineering Conference, Nashville, TN, USA, 25–28 July 2010; p. 6690.
15. Thomas, J.P.; Qidwai, M.A.; Kellogg, J.C. Energy scavenging for small-scale unmanned systems. *J. Power Source* **2006**, *159*, 1494–1509. [CrossRef]
16. Du, T.; Liu, Z.; Sun, X.; Geng, L.; Zhang, X.; An, Y.; Zhang, X.; Wang, K.; Ma, Y. Segmented bi-material cathodes to boost the lithium-ion battery-capacitors. *J. Power Source* **2020**, *478*, 228994. [CrossRef]
17. Hung, J.Y.; Gonzalez, L.F. On parallel hybrid-electric propulsion system for unmanned aerial vehicles. *Prog. Aerosp. Sci.* **2012**, *51*, 1–17. [CrossRef]
18. Ehsani, M.; Gao, Y.; Miller, J.M. Hybrid electric vehicles: Architecture and motor drives. *Proc. IEEE* **2007**, *95*, 719–728. [CrossRef]
19. Ye, X.; Savvarisal, A.; Tsourdos, A.; Zhang, D.; Jason, G. Review of hybrid electric powered aircraft, its conceptual design and energy management methodologies. *Chin. J. Aeronaut.* **2021**, *34*, 432–450.
20. Galkin, B.; Kibilda, J.; DaSilva, L.A. UAVs as mobile infrastructure: Addressing battery lifetime. *IEEE Commun. Mag.* **2019**, *57*, 132–137. [CrossRef]
21. Michini, B.; Toksoz, T.; Redding, J.; Michini, M.; How, J.; Vavrina, M.; Vian, J. Automated battery swap and recharge to enable persistent UAV missions. In Proceedings of the Infotech@ Aerospace 2011, St. Louis, MO, USA, 29–31 March 2011; p. 1405.
22. Gu, B.W.; Choi, S.Y.; Choi, Y.S.; Cai, G.; Seneviratne, L.; Rim, C.T. Novel roaming and stationary tethered aerial robots for continuous mobile missions in nuclear power plants. *Nucl. Eng. Technol.* **2016**, *48*, 982–996. [CrossRef]
23. Dehghan, S.M.M.; Zarezadeh, M.; Farhadian, N.; Moradi, H. The design, modeling and control of a tethered aerial robot for serach and rescue missions. In Proceedings of the 2011 IEEE International Conference on Robotics and Biomimetics, Karon Beach, Thailand, 7–11 December 2011; pp. 1302–1307.
24. Ouyang, J.; Che, Y.; Xu, J.; Wu, K. Throughput maximization for laser-powered UAV wireless communication systems. In Proceedings of the 2018 IEEE International Conference on Communications Workshops (ICC Workshops), Kansas City, MO, USA, 20–24 May 2018; pp. 1–6.
25. Achteik, M.C.; Stumpf, J.; Gurdan, D.; Doth, K.M. Design of a flexible high performance quadcopter platform breaking the MAV endurance record with laser power beaming. In Proceedings of the 2011 IEEE/RSJ International Conference on Intelligent Robots and Systems, San Francisco, CA, USA, 25–30 September 2011; pp. 5166–5172.
26. Yang, Z.; Lei, T.; Lin, Z.; Fu, H.; Zhang, X. The testing platform of hybrid electric power system for a fuel cell unmanned aerial vehicle. In Proceedings of the 2018 IEEE International Conference on Electrical Systems for Aircraft, Railway, Ship Propulsion and Road Vehicles & International Transportation Electrification Conference (ESARS-ITEC), Nottingham, UK, 7–9 November 2018; pp. 1–8.
27. Lee, B.; Park, P.; Kim, C.; Yang, S.; Ahn, S. Power managements of a hybrid electric propulsion system for UAVs. *J. Mech. Sci. Technol.* **2012**, *26*, 2291–2299. [CrossRef]
28. Gang, B.G.; Kwon, S. Design of an energy management technique for high endurance unmanned aerial vehicles powered by fuel and solar cell systems. *Int. J. Hydrogen Energy* **2018**, *43*, 9787–9796. [CrossRef]
29. Koster, J.; Balaban, S.; Hillery, D.; Humbargar, C.; Nasso, D.; Serani, E.; Velazco, A. Design of a blended wing body UAS with hybrid propulsion. In Proceedings of the ASME International Mechanical Engineering Congress and Exposition, Denver, CO, USA, 11–17 November 2011; Volume 54877, pp. 331–337.
30. Gong, A.; Palmer, J.L.; Verstraete, D. Flight test of a fuel-cell/battery/supercapacitor triple hybrid uav propulsion system. In Proceedings of the 31st Congress of the International Council of the Aeronautical Sciences, Belo Horizonte, Brazil, 9–14 September 2018; p. 11.
31. Harvey, J.R.; Jarvis, R.A.; Verstraete, D.; Bagg, R.L.; Honnery, D.; Palmer, J.L. Development of a hybrid-electric power-system model for a small surveillance aircraft. In Proceedings of the 28th International Congress of the Aeronautical Sciences, Brisbane, Australia, 23–28 September 2012.
32. Shiau, J.K.; Ma, D.M.; Yang, P.Y.; Wang, G.F.; Gong, J.H. Design of a solar power management system for an experimental UAV. *IEEE Trans. Aerosp. Electron. Syst.* **2009**, *45*, 1350–1360. [CrossRef]
33. Lu, W.; Zhang, D.; Zhang, J.; Li, T.; Hu, T. Design and implementation of a gasoline-electric hybrid propulsion system for a micro triple tilt-rotor VTOL UAV. In Proceedings of the 2017 6th Data Driven Control and Learning Systems (DDCLS), Chongqing, China, 26–27 May 2017; pp. 433–438.
34. Lin, C.E.; Supsukbaworn, T. Development of dual power multirotor system. *Int. J. Aerosp. Eng.* **2017**, *2017*, 9821401. [CrossRef]
35. Yang, Z.; Lin, F.; Chen, B.M. Survey of autopilot for multi-rotor unmanned aerial vehicles. In Proceedings of the IECON 2016—42nd Annual Conference of the IEEE Industrial Electronics Society, Florence, Italy, 23–26 October 2016; pp. 6122–6127.
36. EVOE10GX2-Manual-EN. Available online: <https://www.horizonhobby.com/pdf/EVOE10GX2-Manual-EN.pdf> (accessed on 11 September 2022).
37. Yadav, S.; Sharma, M.; Borad, A. Thrust efficiency of drones (quadcopter) with different propellers and there payload capacity. *Int. J. Aerosp. Mech. Eng.* **2017**, *4*, 18–23.
38. Leung, S.F.; Zheng, Y.; Choi, C.Y.; Mak, S.S.; Chiu, S.K.; Zee, B.; Mak, A.F. Quantitative measurement of post-irradiation neck fibrosis based on the young modulus: Description of a new method and clinical results. *Cancer Interdiscip. Int. J. Am. Cancer Soc.* **2002**, *95*, 656–662. [CrossRef] [PubMed]

39. Griffis, C.; Wilson, T.; Schneider, J.; Pierpont, P. *Unmanned Aircraft System Propulsion Systems Technology Survey*; Embry-Riddle Aeronautical University: Daytona Beach, FL, USA, 2009.
40. Kortunov, V.; Mazurenko, O.; Gorbenko, A.; Mohammed, W.; Hussein, A. Review and comparative analysis of mini-and micro-UAV autopilots. In Proceedings of the 2015 IEEE International Conference Actual Problems of Unmanned Aerial Vehicles Developments (APUAVD), Kyiv, Ukraine, 13–15 October 2015; pp. 284–289.
41. Series 1580—Thrust Stand and Dynamometer. Available online: <https://www.rcbenchmark.com/dynamometer-series-1580/> (accessed on 11 September 2022).
42. Bershadsky, D.; Haviland, S.; Johnson, E.N. Electric multirotor UAV propulsion system sizing for performance prediction and design optimization. In Proceedings of the 57th AIAA/ASCE/AHS/ASC Structures, Structural Dynamics, and Materials Conference, San Diego, CA, USA, 4–8 January 2016; p. 0581.
43. Fuel Related Products. Available online: <https://fourtituderc.com/collections/fuel-related-products> (accessed on 11 September 2022).
44. Matrice 100—Product Information—DJI. Available online: <https://www.dji.com/matrice100/info#specs> (accessed on 1 November 2022).
45. Xfold Rigs Travel X8 Octocopter (RTF). Available online: [https://www.bhphotovideo.com/c/product/1233282-REG/xfold\\_rigs\\_travel\\_8urtf\\_travel\\_x8\\_u5\\_rtf.html/specs](https://www.bhphotovideo.com/c/product/1233282-REG/xfold_rigs_travel_8urtf_travel_x8_u5_rtf.html/specs) (accessed on 1 November 2022).
46. Inspire 2—Product Information—DJI. Available online: <https://www.dji.com/inspire-2/info#specs> (accessed on 1 November 2022).
47. Thor X4—Professional UAV by Aerial Technology: AeroExpo. Available online: <https://www.aeroexpo.online/prod/aerial-technology/product-181479-18793.html> (accessed on 1 November 2022).